

The detailed nature of active central cluster galaxies

S. I. Loubser

Centre for Space Research, North-West University, Potchefstroom 2520, South Africa

E-mail: Ilani.Loubser@nwu.ac.za

Abstract. We present detailed integral field unit (IFU) observations of the central few kiloparsecs of the ionised nebulae surrounding four active central cluster galaxies (CCGs) in cooling flow clusters (Abell 0496, 0780, 1644 and 2052). Our sample consists of CCGs with H α filaments, and have existing data from the X-ray to radio wavelength regimes available, but lacked the detailed optical emission-line (and simultaneous absorption line) data over a broad wavelength range to probe the dominant ionisation processes, excitation sources, morphology and kinematics of the hot gas (as well as the morphology and kinematics of the stars). This, combined with the other multiwavelength data, will form a complete view of the different phases (hot and cold gas and stars) and how they interact in the processes of star formation and feedback detected in central galaxies in cooling flow clusters, as well as the influence of the host cluster. Here, in this proceedings, we will introduce the observations and derive the optical dust extinction maps of the four nebulae.

1. Introduction

Decades ago, elliptical galaxies were thought to contain very little, if any, gas. Studies of galaxy formation, therefore, often focussed on the stellar properties, however we now know that a large fraction of the baryonic mass in massive galaxies is believed to be in diffuse form. Thus a complete view of galaxy formation necessarily incorporates both the stars and hot gas and an understanding of the processes by which these phases interact (McCarthy et al. 2010).

Cooling-flow clusters are common in the local Universe and massive central cluster galaxies (CCGs) are often found at the centres of these systems (Edwards et al. 2007). If the central cluster density is high enough, intracluster gas can condense and form stars at the bottom of the potential well. Since the radiative cooling times for intracluster gas are short enough that gas can cool and settle to the cluster centre (Edge, Stewart & Fabian 1992), it has been suggested that cD envelopes may arise from the gradual deposition of this cool gas. The lack of widespread detection of iron lines expected from cluster gas cooling below 1 – 2 keV in *XMM-Newton* observations of cool-core clusters contradicted the model that these young stars are formed in cooling flows. However, it is possible that star formation is ongoing in cool-core clusters at a much reduced rate (Bildfell et al. 2008).

Previous studies have reported several examples of ongoing star formation in CCGs, in particular those hosted by cooling-flow clusters (Crawford et al. 1999; Edwards et al. 2007; Bildfell et al. 2008; Loubser et al. 2009). However, the origin of the gas fuelling this star formation is not yet known. Possible explanations include processes involving cooling flows or cold gas deposited during a merging event (Bildfell et al. 2008). These processes will leave different imprints in the dynamical properties, the detailed chemical abundances, and the star formation

Object	Cluster	Redshift z	Linear scale (kpc/arcsec)	R_{off} (Mpc)	Exposure Time (seconds)	Foreground extinction (mag) $E(B-V)_{gal}$
MCG-02-12-039	Abell 0496	0.0329	0.654	0.031	7×1800	0.140
PGC026269	Abell 0780	0.0539	1.059	0.015	6×1800	0.042
PGC044257	Abell 1644	0.0474	0.935	0.009	6×1800	0.071
UGC09799	Abell 2052	0.0345	0.685	0.038	6×1800	0.037

Table 1. CCGs observed with the GMOS-IFU on the Gemini South telescope. All four galaxies show extended $H\alpha$ emission (McDonald et al. 2010). The values for R_{off} (the projected distance between the centre of the optical CCG and the X-ray peak of the cluster) are from Edwards et al. (2007), with the exception of PGC044257 which is from Peres et al. (1998).

histories of these galaxies, which can be studied using high-quality spectroscopy (Loubser et al. 2008; 2012).

As cooling flow models predict more cooled gas than is observed (Bohringer et al. 2001), it is possible that the mass deposited into the molecular clouds is heated by one of several processes - hot young stellar populations, radio-loud AGN, X-rays or heat conduction from the intracluster medium itself, shocks and turbulent mixing layers, and cosmic rays. Therefore, only a small fraction of the cooled gas is detected (Crawford et al. 2005). Thus, CCGs lie at the interface where it is crucial to understand the role of feedback and accretion in star formation. Within these cooling-flow CCGs, cool molecular clouds, warm ionized hydrogen, and the cooling intracluster medium are related. A complete view of the star formation process incorporates the stars with the gas and an understanding of the processes by which these phases interact, and therefore, requires information from several wavelength regimes.

2. Sample

We have chosen our sample of active CCGs from the $H\alpha$ imaging presented in McDonald et al. (2010). From their 23 cooling flow clusters, we selected all the clusters with clearly detected $H\alpha$ in their centres (albeit filamentary, extended or nuclear emission). In addition, all of these central galaxies have optical imaging, near-IR (2MASS) and UV (Galaxy data) available. Thereafter, we selected all the central galaxies with detailed X-ray (Chandra) data, as well as VLA 1.4 GHz fluxes, available. This resulted in a sub-sample of 10 galaxies. The four of these galaxies that we observed with the GMOS IFU are shown in Figure 1.

The rest-wavelength range of the emission lines of interest is 4860–6720 Å ($H\beta$ to $[SII]\lambda 6720$). The ratio of the forbidden $[NII]\lambda 6584$ to $H\alpha$ line will depend on the metallicity of the gas, the form of the ionising radiation, and the star formation rate. The relative strength of the $[OIII]\lambda 5007$ and $H\beta$ lines reveals further excitation mechanism and gas metallicity information. The role of AGN photo-ionisation is confined to the central 2 – 3 arcsec of active, massive elliptical galaxies (Sarzi et al. 2006). Thus, IFU observations are ideal and will also allow us to study the 2D-distribution of the ionising radiation. In addition to the information from the emission lines, we are able to extract the underlying stellar absorption spectra using the improved GANDALF code (Sarzi et al. 2006). Thus, the kinematics and morphology of the hot ionised gas and stellar components can be correlated. The amount of new stars in the CCGs can be quantified using stellar population models, and be directly comparing to the cooling flows in the clusters.

3. Observations and data reduction

The data were obtained with the GMOS-IFU on the Gemini South telescope in semester 2011A (February to July 2011). The GMOS-IFU in 1-slit mode was used and allowed us to map at least a 3 kpc wide region in the centre of the target galaxies with a simultaneous coverage of

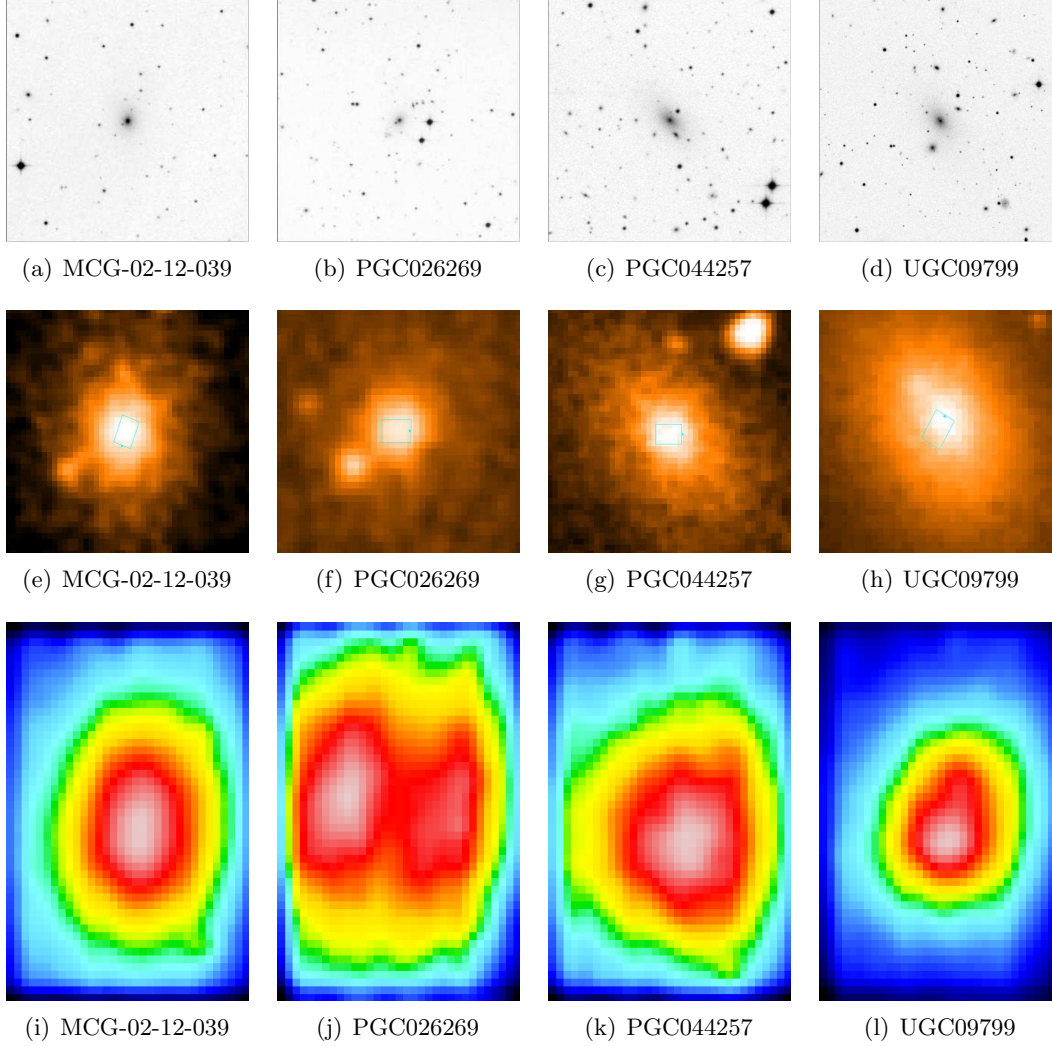


Figure 1. DSS images of the four targets (east to the left). The upper plots show 8×8 arcmin field-of-views (FoV), and the middle plots show the targets with the 5×3.5 arcsec IFU FoV overlaid. The images are orientated with North at the top and East left, and the top of the IFU FoV is indicated with a blue arrow. The lower plots show continuum images made from the IFU cubes (width of 50 \AA at 6350 \AA), smoothed spatially with a Gaussian with width 3 spaxels (which corresponds to 0.3 arcsec) and using the SAURON colourmap.

the $4600\text{--}6800 \text{ \AA}$ range in the target rest frame (using the B600 grating) with a single pointing. Detailed observation and data reduction procedures will be given in Loubser et al. (in prep).

The reduced 2D data arrays were transformed back to a physical coordinate grid (x, y, λ datacube) before scientific analysis, while also correcting for atmospheric dispersion. The latter causes the position of a target within the IFU field to vary with wavelength. This correction was necessary as data were taken at different airmasses throughout the observing nights. Each hexagonal spaxel (spatial element) was 0.2 arcsec , and this was subsampled onto a rectangular grid of 0.1 arcsec per spaxel when the separate exposures were combined. The exposures were combined using a centroid algorithm to calculate the shifting in x and y , and also shifting in λ for the exposures at two different wavelength settings. The cubes were also converted into RSS (row-stacked spectra) for further data reductions in IDL (Interactive Data Language). Each

spaxel was averaged with its eight neighbouring spaxels, which is effectively smoothing over 0.3 arcsecs - this is still slightly undersampled compared to the average seeing, but only larger regions will be analysed further.

4. Line measurements and internal extinction

To accurately measure the emission-line fluxes of the CCG spectra, we use a combination of the PPF (Cappellari & Emsellem 2004) and GANDALF (Sarzi et al. 2006) routines¹. Gandalf version 1.5 was used as it enables a reddening correction to be performed, and it incorporates errors. This code treats the emission lines as additional Gaussian templates, and solves linearly at each step for their amplitudes and the optimal combination of stellar templates, which are convolved by the best stellar line-of-sight velocity distribution. The stellar continuum and emission lines are fitted simultaneously. All 985 stars of the MILES stellar library (Sánchez-Blázquez et al. 2006) were used as stellar templates to automatically include α -enhancement in the derived optimal template. The $H\alpha$ and $[\text{NII}]\lambda 6583$ lines were fitted first, and the kinematics of all the other lines were tied to these lines, following the procedure described in Sarzi et al. (2006). However, in cases where the emission of the other lines (example $H\beta$) were strong enough to measure velocity and velocity dispersion, this was calculated independently as there is no a priori reason to expect the kinematics measured from the $[\text{NII}]\lambda 6583$ and $H\beta$ lines to be the same (as they can originate in different regions). After the kinematics are fixed, a Gaussian template is constructed for each emission line at each iteration, and the best linear combination of both stellar and emission-line templates (with positive weights) is determined. This is done without assuming line ratios, except in the case of doublets where their relative strength is fixed by the ratio of the corresponding transition probabilities. We have adapted the GANDALF code to apply it to the GMOS-IFU cubes for a longer wavelength range. All 1617 spaxels were collapsed together to obtain a 1D spectrum per cube, thereafter all 985 stars for the MILES library were used to create a global optimal template for each galaxy. This global optimal template (and the stars it consisted of – to account for varying weights over the spatial region) was then applied to all 1617 spectra per cube.

Some ellipticals contain dust in the centre that can be patchy, uniform or filamentary (Laine et al. 2003). The long wavelength range of the spectra allows GANDALF to constrain the amount of reddening using the observed decrement of the Balmer lines, which can be set to have an intrinsic decrement consistent with the recombination theory by treating the lines as a multiplet. The physical constraints on the emission from the higher-order Balmer lines also ensures the strength of the corresponding absorption features is correctly estimated.

It uses the dust models by Calzetti et al. (2000) to return the flux attenuation values at the desired wavelength for any given $E(B - V)$ value (optional, see below). The Balmer decrement assumes a case B recombination for a density of 100 cm^{-3} and a temperature of 10^4 K , resulting in the predicted $H\alpha/H\beta$ ratio of 2.86 (Osterbrock 1989). The code can adopt either a single dust component, affecting both the stellar continuum and the emission-line fluxes, or include a second dust component that affects only the emission-line templates.

The parameter $E(B - V)$, i.e. the colour excess between 4350 \AA and 5550 \AA , for the galactic extinction for each of the four galaxies was taken from the NED database (Schlegel, Finkbeiner & Davis 1998), and ranged between 0.037 and 0.140 mag. The parameter R_V , i.e. the ratio of the absolute extinction at 5550 \AA (A_V) to the colour excess $E(B - V)$, was taken as 3.1 for the interstellar medium (Cardelli, Clayton & Mathis 1989). The total extinction is then given by:

$$E(B - V)_{total} = \frac{2.177}{-0.37R} \times \left(\log \frac{I_{0H\alpha}}{I_{0H\beta}} - \log \frac{I_{H\alpha}}{I_{H\beta}} \right)$$

¹ We make use of the corresponding PPF and GANDALF IDL codes which can be retrieved at <http://www.leidenuniv.nl/sauron/>.

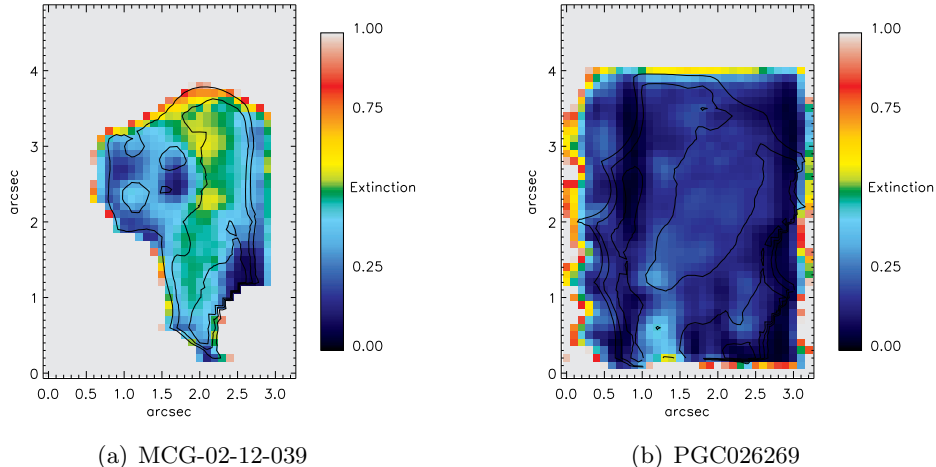


Figure 2. Total extinction of MCG-02-12-039 and PGC026269. The extinction was smoothed over 0.3 arcseconds, and is only plotted where the velocity dispersion of the $H\alpha$ line is less than 500 km s^{-1} (to avoid spaxels where the $H\alpha$ line could not be separated from the NII lines), and it is only plotted where the A/N ratio of the $H\alpha$ line is higher than 3. The $H\alpha$ flux contours are overplotted at 1 magnitude apart.

The theoretical $H\alpha/H\beta$ flux ratio of 2.86 may not be the ideal value to use for Seyfert-type galaxies, but the actual value is debated. It is often assumed that the $H\alpha$ emission in these systems is enhanced due to collisional processes, and several authors use a value R_V of 3.1 (Osterbrock 1989), although other values have also been determined (Binette et al. 1990 calculate a value of 3.4). The total extinction measured from the Balmer decrement are shown in Figures 2 and 3. The extinction was smoothed over 0.3 arcseconds, and is only plotted where the velocity dispersion of the $H\alpha$ line is less than 500 km s^{-1} (to avoid spaxels where the $H\alpha$ line could not be separated from the bordering NII lines), and it is only plotted where the amplitude-to-noise (A/N) ratio of the $H\alpha$ line is higher than 3 (as defined in Sarzi et al. (2006).

Figures 2 and 3 and shows very low extinction mostly, but some morphological features can be seen in MCG-02-12-039 and UGC09799. In particular, high values of $E(B - V)_{internal}$ can be seen in UGC09799 (once $E(B - V)_{gal}$ (Table 1) is subtracted from $E(B - V)_{total}$ (given in the maps)). The galactic extinction of PGC044257 is $E(B - V)_{gal} = 0.071 \text{ mag}$, and from long-slit spectra, Crawford et al. (1999) derived the total extinction as 0.46 to 0.63 mag. This agrees with the extinction we derived for the very centre of the galaxy in Figure 3, but on average our spatially resolved extinction is slightly lower. The galactic extinction $E(B - V)_{gal}$ of UGC09799 is 0.037 mag, and Crawford et al. (1999) derived an integrated internal extinction of $E(B - V)$ of 0.22 mag for the centre of this galaxy. This corresponds very well to what we derived and plotted in Figure 3, although we find that some regions shows much higher internal extinction. The values of extinction determined here may be slightly overestimated due to the choice of intrinsic $H\alpha/H\beta$ flux used.

5. Future work

We are currently measuring the kinematics of the gas and stellar components, and correlating them with each other. Now that we can also measure reddening-corrected fluxes, we can also derive the line ratios to help us determine the ionisation mechanisms. We are continuing the observational program, and a further five of the ten galaxies in the subsample (with confirmed $H\alpha$ emission and detailed auxillary data already available) have already been observed with

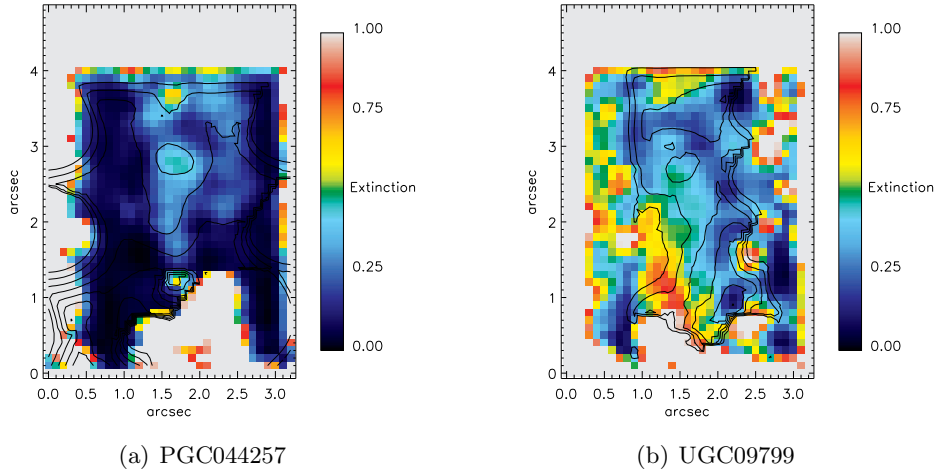


Figure 3. Total extinction of PGC044257 and UGC09799. See caption of Figure 2 for explanation.

long-slit spectroscopy on SALT (the Southern African Large Telescope).

Acknowledgments

SIL is financially supported by the South African National Research Foundation. Based on observations obtained on the Gemini South telescope.

References

- [1] Bildfell C, Hoekstra H, Babul A and Mahdavi A 2008 *MNRAS* **389** 1637
- [2] Binette L, Raga A C, Calvet N and Canto J 1990 *PASP* **102** 723
- [3] Bohringer H et al 2001 *A&A* **365** 181
- [4] Calzetti D, Armus L, Bohlin R C, Kinney A L, Koornneef J and Storchi-Bergmann T 2000 *ApJ* **533** 682
- [5] Cappellari M and Emsellem E 2004 *PASP* **116** 138
- [6] Cardelli J A, Clayton G C and Mathis J S 1989 *ApJ* **345** 245
- [7] Crawford C S, Allen S W, Ebeling H, Edge A C and Fabian A C 1999 *MNRAS* **306** 857
- [8] Crawford C S, Hatch N A, Fabian A C and Sanders J S 2005 *MNRAS* **363** 216
- [9] Edge A C, Stewart G C and Fabian A C 1992 *MNRAS* **258** 177
- [10] Edwards L O V, Hudson M J, Balogh M L and Smith R J 2007 *MNRAS* **379** 100
- [11] Laine S, Van der Marel R P, Lauer T R, Postman M, O’Dea C P and Owen F N 2003 *AJ* **125** 478
- [12] Loubser S I, Sansom A E, Sánchez-Blázquez, P Soechting I K and Bromage G 2008 *MNRAS* **391** 1009
- [13] Loubser S I, Sánchez-Blázquez P, Sansom A E and Soechting I K 2009 *MNRAS* **398** 133
- [14] Loubser S I and Sánchez-Blázquez P 2012 *MNRAS* **in print**
- [15] McCarthy I G et al 2010 *MNRAS* **406** 822
- [16] McDonald M, Veilleux S, Rupke D S N and Mushotzky R 2010 *ApJ* **721** 1262
- [17] Osterbrock D E 1989 *Astrophysics of gaseous nebulae and active galactic nuclei* (University Science Books, Mill Valley CA)
- [18] Peres C B, Fabian A C, Edge A C, Allen S W, Johnstone R M and White D A 1998 *MNRAS* **298** 416
- [19] Sánchez-Blázquez P et al 2006 *MNRAS* **371** 703
- [20] Sarzi M et al 2006 *MNRAS* **366** 1151
- [21] Schlegel D J, Finkbeiner D P and Davis M 1998 *ApJ* **500** 525